

Nanoscale

Accepted Manuscript



This is an *Accepted Manuscript*, which has been through the Royal Society of Chemistry peer review process and has been accepted for publication.

Accepted Manuscripts are published online shortly after acceptance, before technical editing, formatting and proof reading. Using this free service, authors can make their results available to the community, in citable form, before we publish the edited article. We will replace this *Accepted Manuscript* with the edited and formatted *Advance Article* as soon as it is available.

You can find more information about *Accepted Manuscripts* in the [Information for Authors](#).

Please note that technical editing may introduce minor changes to the text and/or graphics, which may alter content. The journal's standard [Terms & Conditions](#) and the [Ethical guidelines](#) still apply. In no event shall the Royal Society of Chemistry be held responsible for any errors or omissions in this *Accepted Manuscript* or any consequences arising from the use of any information it contains.

A BIOCOMPATIBILITY STUDY OF NEW NANOFIBROUS SCAFFOLDS FOR NERVOUS REGENERATION

A. Raspa^{a,b}, A. Marchini^a, R. Pugliese^{a,b}, M. Mauri^c, M. Maleki^{a,b}, R. Vasita^d and F. Gelain^{a,b}

^a Center for Nanomedicine and Tissue Engineering (CNTE), A.O. Ospedale Niguarda Cà Granda, Piazza dell'ospedale maggiore 3, 20162 Milan, Italy. E-mail: gelain@mit.edu; Fax: +39 02 87073821; Tel.: +39 02 64447527

^b IRCCS Casa Sollievo della Sofferenza, Opera di San Pio da Pietrelcina, Viale Cappuccini 1 San Giovanni Rotondo (FG) 71013, Italy

^c Dipartimento di Scienza dei Materiali, Università degli Studi di Milano Bicocca, Via Roberto Cozzi, 55, 20125 Milano, Italy

^d School of Life Sciences, Central University of Gujarat, Sector-30, Gandhinagar-382030, Gujarat, India

† Electronic supplementary information (ESI) available: *In vivo* analysis to evaluate tissue reaction in the scaffold implant walls (Fig. S1) and to test axonal regeneration (Fig. S2). Waters LC-MS Alliance -3100 analysis to confirm the molecular weight and the integrity of peptide following the electrospray process (Fig. S3). Water Contact Angle of electrospun nanofibrous mats (Fig. S4).

ABSTRACT

The development of therapeutic approaches for Spinal cord injury (SCI) is still a challenging goal to be achieved. The pathophysiological features of chronic SCI are glial scar and cavity formation: an effective therapy will require contribution of different disciplines such as materials science, cell biology, drug delivery and nanotechnology. One of the biggest challenges in SCI regeneration is to create an artificial scaffold that could mimic the extracellular matrix (ECM) and support nervous regeneration. Electrospun constructs and hydrogels based on self-assembling peptides (SAPs) have been recently preferred. In this work SAPs and polymers were assembled by using a coaxial electrospinning setup. We tested the biocompatibility of two types of coaxially electrospun microchannels: the first one made by a core of poly(ϵ -caprolactone) and poly(D,L-lactide-co-glycolide) (PCL-PLGA) and a shell of an emulsion of PCL-PLGA and functionalized self-assembling peptide Ac-FAQ and the second one made by a core of Ac-FAQ and a shell of PCL-PLGA. Moreover, we tested an annealed scaffold by PCL-PLGA microchannel heat-treating. The properties of coaxial scaffolds were analyzed with Scanning electron microscope (SEM), Fourier transform spectroscopy (FTIR), Contact angle and differential scanning calorimetry (DSC). *In vitro* cytotoxicity was assessed via viability and differentiation assays with neural stem cells (NSC); whereas *in vivo* inflammatory response was evaluated following scaffold implantation in rodent spinal cords. Emulsification of the outer shell turned out to be the best choice in terms of cell viability and tissue response: thus suggesting the potential of using functionalized SAPs in coaxial electrospinning for regenerative medicine applications.

1. Introduction

Spinal Cord Injury (SCI) in adult mammals causes an initial physical trauma followed by a secondary process of tissue destruction arising from robust and persistent inflammatory responses, ischemia, edema, and demyelination¹ resulting in the development of large zones of necrosis at the site of injury, ultimately creating cavities that prevent communication between brain and spinal cord.

In order to recover spinal functionality, it is crucial to regenerate the lost tissue at least partially. Tissue engineered scaffolding, aimed at mimicking the native extracellular matrix (ECM), is an increasingly popular strategy for the treatment of SCI². In fact, neural tissue ECM consists of aligned collagen-based fibers, whose fiber/fibril diameter and alignment encourages the guided growth neural cells.

The ability to synthesize nanofibrous scaffolds in shape of conduits or of aligned microfibers using electrospinning technique has increased the possible applications in neural tissue engineering. Nonetheless, these scaffolds must be deeply characterized in order to control and optimize their final properties and, among them, biocompatibility. Biomaterials designed for spinal cord repair should provoke minimal chronic inflammation and immune responses when implanted in the Central Nervous System (CNS)^{3,4}.

Among others, in chronic and acute SCI, various efforts have been focused on designing new biomaterials capable of stimulating and promoting sensory and motor axonal regeneration when delivered at the site of injury by providing permissive microenvironments mimicking the native ECM⁵. In this regard, biodegradable electrospun scaffolds based on aliphatic polyester, such as poly(D,L-lactide-co-glycolide) (PLGA) and poly(ϵ -caprolactone) (PCL), have been widely studied for various biomedical applications^{6,7} due to their biocompatibility, biodegradability, excellent fiber-forming properties^{8,9} and their approval by Food and Drug Administration (FDA) for clinical usage.

PCL electrospun nanofibers have good mechanical strength but also a prolonged biodegradation profile, making them unsuited for neural implantation where scaffold remains may hamper tissue regeneration. Moreover, its inert nature can affect protein adsorption eventually yielding to unfavorable cell adhesion sites. On the other hand, injectable scaffolds, made of SAPs, belong to the hydrogel family and show a remarkable regenerative potential because of their good biocompatibility, tailorability for slow drug release and, most importantly, easy functionalization with bioactive motifs^{10,11}. Thus, despite the large numbers of synthetic polymer-based scaffolds, self-assembling peptides (SAPs) are still the preferred choice for SCI regenerative therapies. In our previous publication a SAP named Ac-FAQ (Ac-FAQRVPP-GGG-(LDLK)₃-CONH₂), selected also in this work, demonstrated significant locomotor recovery when injected in acutely SCI in rats: it did not alter the physiological inflammatory response and enhanced neural regeneration¹².

Several studies have explored the usage of electrospun nanofibrous scaffold to guide neural cell growth^{13,14}. Combination of SAPs with electrospun fibers could be the next promising step for neural prostheses. Blended PCL-PLGA with biological active peptide sequences may presumably not only change the electrospun scaffold surface properties but also enhance the regeneration process at the site of implant. The integration of bioactive SAPs with polymeric nanofibers will immobilize SAPs for longer time

whereas nanofibers will provide substrate for guided cell growth. In current study, SAPs and polymers were integrated by using a coaxial electrospinning setup by itself or by using, in addition to that, emulsified solutions of the two together. The core-shell scaffolds allow for encapsulation of biologically active molecules despite of the different solvent systems used for spinning the two solutions¹⁵⁻¹⁹. Moreover, coaxial arrangement enhanced the loading capacity, reduced the loss of bioactivity and demonstrated sustained release of biomolecules from core^{16,17}.

Briefly, we introduced here and tested two types of SAP encapsulated PCL-PLGA coaxial electrospun scaffolds: one having Ac-FAQ in the core and PCL-PLGA in the shell and the other containing an emulsion of PCL-PLGA with Ac-FAQ in the shell and PCL-PLGA in the core. We also tested a thermally Annealed PCL-PLGA microchannel to assess the effects of scaffold fused fibers and decreased porosity on the overall biocompatibility and on the likely decreased ectopic cell infiltration.

The physical and chemical properties of coaxial scaffolds were analyzed with Scanning electron microscope (SEM), Fourier transform spectroscopy (FTIR), Contact angle and differential scanning calorimetry (DSC). These studies pointed out the nanofibrous nature of scaffolds and minuscule alteration in surface and bulk properties of PCL-PLGA nanofibers. Cytotoxicity was evaluated via *in vitro* viability and differentiation assays of neural stem cells (NSC). Furthermore, *in vivo* studies were conducted to evaluate inflammatory response following scaffolds implantation in rodent spinal cords, examining the distribution of activated macrophages/microglia and reactive astrocytes response.

In vitro experiments the scaffolds featuring nanofiber shells of PCL-PLGA emulsified with Ac-FAQ were demonstrated to be comparable to positive control, while in *in vivo* experiments most of the implanted scaffolds showed values of immune reaction similar to sham-operated group; thus suggesting that the core-shell electrospun scaffolds mixed with SAPs may be promising implants to be adopted in the field of nervous regeneration.

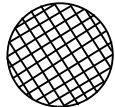
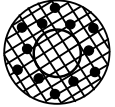
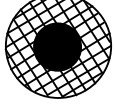
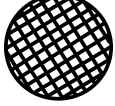
2. Results:

2.1 Fiber preparation and characterization

In the current study PCL-PLGA was combined with 1% w/v of Ac-FAQ with the objective of enhancing the bioactivity of implants. Two types of PCL-PLGA/peptide nanofibers were electrospun and are shown in Table 1. In all samples fiber orientation was random with an average fiber diameter of 600 nm and a diameter range of 200-1000 nm. Scanning electron micrographs (Fig. 1a) revealed continuous and smooth morphology with no perceivable difference between Coaxial I and Coaxial II.

The Annealed sample instead presents thicker fibers and beads due to partial melting and agglomeration of the fibers during annealing at 60°C. This temperature is slightly below the melting point of PCL and reduces sample porosity without disrupting the shape of the implantable microchannel: thus we could single out the effect of the nanostructure on the infiltration of inflammatory cells within the implanted scaffold.

Table 1 Scheme of fiber typology used.

SAMPLE	JET	CORE	SHELL	STRUCTURE
BLEND	SINGLE	NO	NO	
COAXIAL I	COAXIAL	PCL – PLGA	EMULSION PCL – PLGA WITH Ac-FAQ	
COAXIAL II	COAXIAL	Ac-FAQ	PCL – PLGA	
ANNEALED	SINGLE	NO	NO	

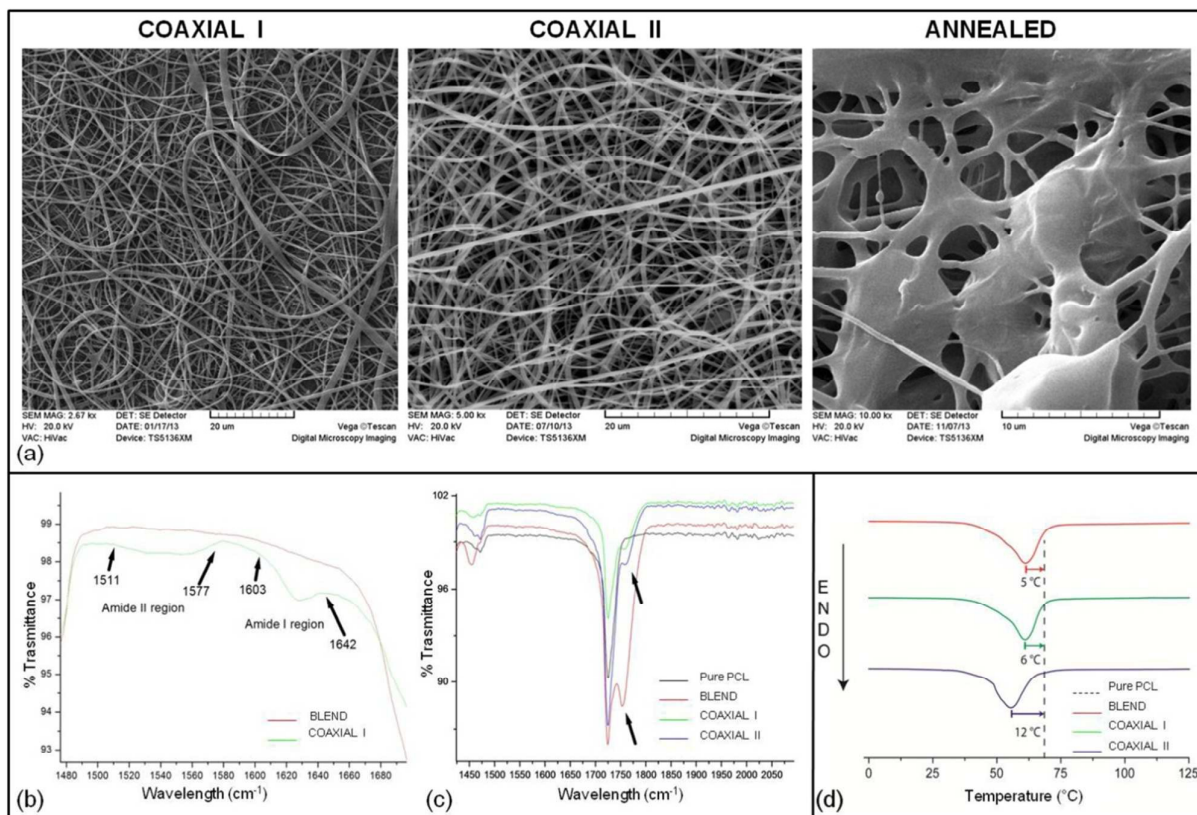


Figure 1 (a) Scanning electron micrographs of the following tested samples: Coaxial I, Coaxial II and Annealed. FT-infrared spectra of electrospun nanofibrous scaffolds: (b) Amide I & II stretching due to the peptide in Coaxial II, in comparison to Blend. (c) Reduction in C=O stretching spectra from Blend to all other samples. (d) DSC traces recorded during first heating of nanomesh samples, containing information on the stability of the polymer morphologies resulting from each preparation. The reference PCL trace is not shown: its melting point is outlined with the dashed vertical line. Differences in melting point are apparent, with Coaxial II sample presenting a melting peak at 55.5°, whereas Coaxial I and Blend nanofibers both melt around 61 °C, and reference pure PCL melts at 67 °C.

2.2 Water Contact Angle (WCA) measurement

This study was performed to understand the effect of peptide/peptide solution on nanofibrous surface, although low concentrations of peptides were not expected to make any significant change except on nanofibers surface texture due to evaporation of water from emulsion. Statistical analysis showed that no statistically significant difference existed between the wettability of the coaxial I and coaxial II electrospun mats ($p=0.7076$, $\alpha = 0.05$) while the difference is considered to be statistically significant between blend and other samples. As expected marginal increase in contact angles of Coaxial I and Coaxial II fibers have been observed (see Table 2). This marginal increase both on Coaxial I and Coaxial II nanofibers can be attributed to change (decrease) in surface coverage of C=O group because of their anticipated interactions with peptide chains. Furthermore, contact angle of water droplets on nanofibrous meshes was recorded till 5 minutes at 30 seconds interval to study the dynamic contact angle. However, none of samples showed any change in contact angle from first measurement to last measurement. We speculate that incorporation of 1% peptide could not change fiber surface physical properties enough to be detected through this methodology.

Table 2 Water contact angle measurements (°) on electrospun fibrous meshes of Blend, Coaxial I and Coaxial II samples.

Sample Name	Contact angle	
	Left	Right
BLEND	129° ± 1	129° ± 1
COAXIAL I	135° ± 3	135° ± 3
COAXIAL II	134° ± 2	134° ± 2

2.3 FTIR analysis

FTIR spectroscopy was used to identify the change in surface chemistry after blending or co-spinning for peptides with PCL-PLGA nanofibers. The infrared spectrum of Blend sample was to a large extent similar to the spectrum of the Coaxial samples. However, numbers of small peaks belonging to peptides (Amide I and Amide II) and changes in C=O surface coverage have been observed (Fig 1b and c). Most of PCL and PLGA peaks were overlapping except 865 cm^{-1} , which represent PLGA in blend. The presence of PCL was confirmed by 2948 cm^{-1} (C-H stretch), 1725 cm^{-1} (C=O stretch) and 1177 cm^{-1} (C-O stretch). In case of 1755 cm^{-1} peak, which represent C=O stretching, it was shown a significant decrease in intensity for Coaxial samples. This observation can be attributed to the possible interactions between C=O and peptide chains which eventually reduce their exposure on fiber surface.

Another possible region for finding peptide presence on nanofibers surface was Amide I and II peaks at ~ 1618 and ~ 1543 respectively. However, only Coaxial I nanofibers which contain peptide in shell region showed Amide I & II signature peaks. These results clearly indicated that peptides were incorporated into nanofibers.

2.4 Thermal Analysis

Thermal properties of Blend and the PCL-PLGA combined with peptides were investigated by DSC, whose results are reported in Table 3 together with characterization of the raw materials PCL and PLGA. The raw materials display standard thermal properties, thus in Fig 1d only the nanostructured samples are graphically plotted.

For analyzing the phase transition, we considered the two polymers separated at the local scale²⁰, and thus treated the DSC traces as linear combinations of the reference PLGA and PCL weighted by the respective ratios (4:5.5). Thus, after baseline correction the endothermal peak was integrated and the crystallinity χ was measured with the following equation:

$$\chi = \frac{\Delta H_{fus}}{\Delta H_{PCL} * f_{PCL} / (f_{PCL} + F_{PLGA})}$$

Where ΔH_{PCL} is the enthalpy of fusion for fully crystalline PCL, and f_X indicates the weight fraction of the given polymer (PCL or PLGA). The 1% peptide, where present, was neglected in the calculation.

Data acquired during the first and second heating segment of the DSC are separately reported in Table 3: the first scan (Fig. 1d) is most informative of the thermo-mechanical history of each sample and highlights the differences due to the preparation of each nanofibrous mesh. During this first heating, the sample melts and loses its mesh structure: the second scan provides preparation-independent information on the polymers. On first heating the melting points of Blend and Coaxial I are similar, and they are both more than 5 °C lower than the melting point of reference PCL. The Coaxial II sample has a further significant lowering (>5 °C) in melting point relative to Blend and Coaxial I.

Comparison between Blend and Coaxial I indicates that the presence of 1% w/v peptide did not change the structure and thermal properties of the polymer. Instead, the Coaxial II sample presents a significant decrease of the enthalpy, indicating a reduced quality of the crystals, compatible with a system with higher interface, as in the case of “hollow” fibers, or to kinetic reasons like the disruption of forming crystals due to water evaporation, as expected in conditions where the core itself was constituted by water peptide solution (Table 3). As predicted, values measured during the second heating are much less differentiated, since the first heating melts the samples and resets their morphology, erasing the features associated to microfabrication.

Table 3 Differential scanning calorimeter (DSC) analysis of pure PCL and electrospun nanofibrous meshes of Blend, Coaxial I and Coaxial II. Data are separately reported for the two heating segments applied to the two samples. Crystallinity are referred to PCL fraction alone, after baseline correction for the presence of PLGA, and calculated using the value of 136 J/g enthalpy of fusion for fully crystalline PCL.

Sample name	1 st Heating Cycle	ΔH_{fus} J/g	Crystallinity Fraction χ	2 nd Heating segment:	ΔH_{fus} J/g
	Peak (°C)			Peak (°C)	
PCL	67±1	98±6	0.71±0.05	56.5±1	78±7
Blend	61±1	67±6	0.71±0.08	56±1	54±5
Coaxial I	60±1	64±5	0.68±0.07	57±1	48±4
Coaxial II	55.5±0.5	55±4	0.57±0.05	53±1	46±4
PLGA	T _g = 46 °C		0	T _g = 43 °C	

2.5 *In Vitro* results

Cell viability assays are crucial to test the potential of newly developed biomaterials for tissue engineering applications. Also, assessments of cell adhesion, spreading and proliferation give precious info regarding the possible interactions between scaffolds and cells of the host tissues. The functionalized self-assembling peptide Ac-FAQ used in Coaxial I and Coaxial II has already been demonstrated to support NSC growth, yielding to percentages of neurons and oligodendrocytes significantly higher when compared to the progenies cultured on Cultrex¹².

Hence NSC proliferative and differentiating potentials of co-electrospun scaffolds deposited on glass coverslips have been tested *in vitro*. All tests were performed after 7 days *in vitro* (7DIV) and Cultrex coated coverslips were used as positive controls.

MTS assay was performed to determine mNSCs viability on electrospun circular glass coverslips (Fig. 2a): it showed larger populations of viable mNSCs on Coaxial I substrates, indeed no significant difference was detected with Cultrex, while significantly less viable cells were observed on Blend, Coaxial II and Annealed substrates. These results indicate that Coaxial I, comprising the emulsion of Ac-FAQ and PCL-PLGA in the outer shell, was the best choice as for cell proliferation and viability.

Immunofluorescence against post-mitotic neurons (Beta III Tubulin), astrocytes (GFAP) and oligodendrocytes (GalC - O4) was performed for each condition (Fig. 2b and c). mNSCs cultured on scaffolds exhibited neural branching similar to that found on Cultrex. Quantitative results are expressed as a percentage of the total cell population (DAPI cell nuclei staining). In case of Beta III Tubulin the Blend, Coaxial I, Coaxial II and Annealed samples showed respectively 26.53 ± 1.37%, 28.81 ± 2.68%, 30.84 ± 7.84% and 29.25 ± 0.29% of positive cells. In case of Cultrex we detected 19.22 ± 2.34% of cells positive to Beta III Tubulin. Lacking any significant difference among the just mentioned results, the percentage of Beta III Tubulin+ cells were comparable to mNSCs differentiating on Cultrex.

Of all scaffolds tested, Coaxial I and Coaxial II exhibited the highest percentage of positive cells for the astrocytes marker GFAP (46.85 ± 4.28% for Coaxial I; 53.16 ± 11.12% for Coaxial II). These values are similar to those found with Cultrex (61.12 ± 1.89% GFAP+ cells). In case of Blend and Annealed we detected 37.54 ± 4.61% and 43.33 ± 4.40% of cells positive to GFAP: values significantly lower than Cultrex.

On the other hand, the percentage of oligodendrocytes of mNSCs on Blend, Coaxial I, Coaxial II and Annealed were respectively $11.35 \pm 0.74\%$, $18.32 \pm 4.83\%$, $21.52 \pm 4.04\%$ and $25.74 \pm 2.92\%$. Statistical analysis pointed out significant differences of GalC/O4+ murine cells on Cultrex ($21.48 \pm 3.27\%$) vs Blend, while all other substrates gave data comparable to Cultrex.

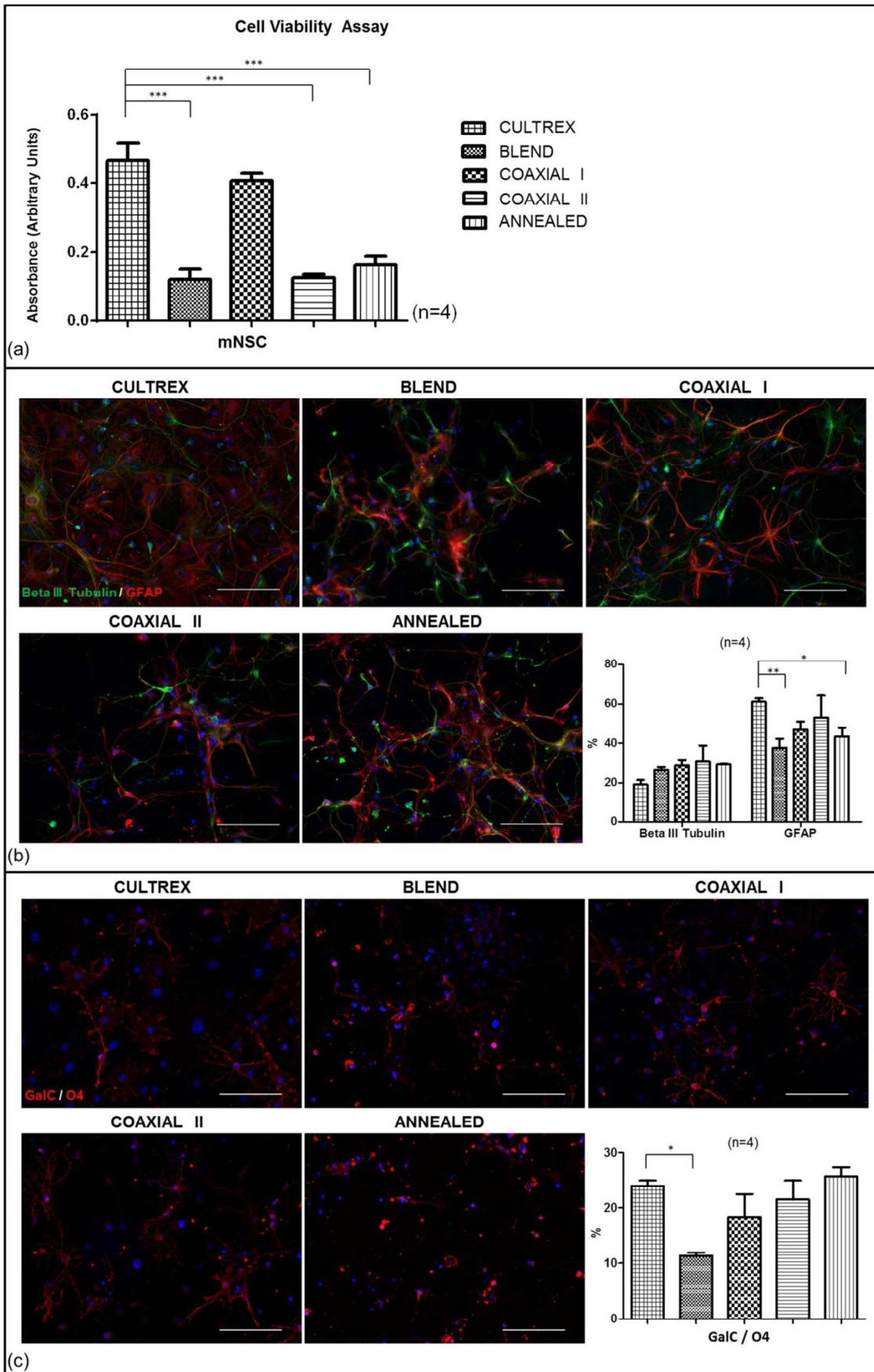


Figure 2 *In vitro* study: (a) MTS assay for cell viability of mNSCs cultured on Cultrex, Blend, Coaxial I, Coaxial II and Annealed scaffolds at 7 DIV. Results point out significant differences between Blend, Coaxial II and Annealed vs Cultrex ($*** p < 0.001$). No significant difference was detected between Cultrex and Coaxial I. Cell nuclei are visualized with DAPI (blue). (b) Neural/astroglial differentiation assessment: quantification of mNSCs differentiation shows no significant differences between all scaffolds and Cultrex for Beta III Tubulin+ (green) cells, while there are significant differences among Blend and Annealed scaffolds vs Cultrex for GFAP+ (red) cells ($** p < 0.01$; $* p < 0.05$). (c) Oligodendroglial differentiation assessment: quantification of GalC/O4+ cells (red) shows significant difference between Blend vs Cultrex ($*p < 0.05$). Scale bars = 100 μm .

2.6 *In vivo* results

To evaluate the host tissue reaction to the implanted electrospun scaffolds they were inserted intramedullary into rats and processed after one month (see methods section for details). We examined the implants, stub wounds and the surrounding spinal cord tissues. We determined the effect of scaffolds on inflammatory cell activation by histological analysis. We evaluated the cell density of IBA1+ and CD68+ cells in the spinal cord tissue surrounding (Fig. 3a) and within the implants (See ESI and Fig. S1† for details).

IBA1 is a microglia/macrophage-specific calcium-binding protein: IBA1+ cell density in Sham-operated animals was 486.2685 ± 51.485 cells/ mm^2 ; while the average number of IBA1+ cells in tissues receiving the scaffolds were 125.3480 ± 13.031 cells/ mm^2 , 314.3095 ± 27.128 cells/ mm^2 , 598.8207 ± 53.163 cells/ mm^2 , 383.8618 ± 27.751 cells/ mm^2 for tissues surrounding respectively Blend, Coaxial I, Coaxial II and Annealed implants (Fig. 3a). The microglial response for all scaffolds was significantly different depending on the type of implanted scaffolds. At 1 month, Blend and Coaxial I scaffolds had fewer IBA1+ cells at the implant site than Sham-operated animals ($*** p < 0.001$, Sham vs Blend; $** p < 0.01$, Sham vs Coaxial I). Density of IBA1+ cells in Coaxial II and Annealed group animals seems having no significant differences in respect to Sham group, although between Coaxial II vs Annealed there was a considerable difference ($^{sss} p < 0.001$). The number of IBA1+ cells for Blend scaffolds was very low, showing significant difference compared to all other scaffolds ($^{++} p < 0.01$, Blend vs Coaxial I; $^{+++} p < 0.001$, Blend vs Coaxial II; $^{+++} p < 0.001$, Blend vs Annealed). Finally, significant differences between Coaxial I and Coaxial II groups were detected ($^{sss} p < 0.001$).

On the other hand the number of CD68+ cells was lower in all animals receiving implants. CD68+ cells were 311.9259 ± 33.014 cells/ mm^2 in Sham-operated group; 34.7812 ± 4.453 cells/ mm^2 in Blend group; 192.9280 ± 19.604 cells/ mm^2 in Coaxial I group; 285.2787 ± 37.598 cells/ mm^2 in Coaxial II group; 270.3423 ± 20.559 cells/ mm^2 in Annealed group. Statistical analysis showed significant differences between Blend and Coaxial I vs Sham ($*** p < 0.001$ and $* p < 0.05$ respectively), Coaxial I vs Blend ($^{++} p < 0.01$), and lastly Coaxial II and Annealed vs Blend ($^{+++} p < 0.001$).

We also measured the cell density of IBA1+ and CD68+ cells within the walls of implanted microchannels (see ESI and Fig S1† for details). IBA1+ cells were 268.2055 ± 71.214 cells/ mm^2 in Blend group; 241.1217 ± 71.631 in Coaxial I; 230.2426 ± 58.503 cells/ mm^2 in Coaxial II; 39.7989 ± 17.014 in Annealed animals. In this case statistical analysis showed similar results in almost all scaffolds giving no significance differences, except for Annealed that had the lowest density of IBA1+ cells ($* p < 0.05$ Annealed vs Blend, Coaxial I and Coaxial II). Again, in case of CD68 the cell density is smaller than IBA1+ cells. The results calculated for channel

walls showed: 157.6573 ± 37.085 CD68 + cells/mm² in Blend; 61.9298 ± 17.059 cells/mm² in Coaxial I; 82.3591 ± 20.536 cells/mm² in Coaxial II; lastly 9.3980 ± 2.654 cells/mm² in Annealed. Statistical analysis showed no significance differences in terms of CD68+ cells infiltrated into the walls of all scaffolds.

GFAP staining showed reactive astrocytosis surrounding each implant at 1 month (Fig. 3b): GFAP were presents at the borders of the scaffold areas, forming an intense glial border. Their response occurs often later than the microglial one and is associated with a cytotropic process. GFAP immunoreactivity was 0.0250 ± 0.002 mm², 0.0325 ± 0.006 mm², 0.0227 ± 0.002 mm², 0.0416 ± 0.006 mm², 0.0228 ± 0.002 mm² respectively in Sham-operated, Blend, Coaxial I, Coaxial II and Annealed experimental groups.

We also tested the implantation site for the reactivity against Fibroblast and Collagen IV markers (Fig 3c). Fibroblasts play an essential role in the synthesis of all collagens and, in particular, of Collagen IV, one of the main components of basement membrane in the nervous tissue. Averaged reactivity area for Fibroblasts in Sham-operated animals was 0.0285 ± 0.003 mm², whereas it was 0.0147 ± 0.003 mm², 0.0209 ± 0.005 mm², 0.0251 ± 0.003 mm², 0.0164 ± 0.006 mm² respectively in Blend, Coaxial I, Coaxial II and Annealed experimental groups. No significant difference was observed. On the other hand the averaged reactivity area for Collagen IV was 0.0507 ± 0.012 mm² in Sham operated animals; 0.0227 ± 0.003 in Blend experimental group; 0.0364 ± 0.005 in Coaxial I; 0.0426 ± 0.007 in Coaxial II and 0.0260 ± 0.005 in animals receiving Annealed scaffolds. Results show significantly greater reactivity of Collagen IV in Sham group in comparison with Annealed and Blend group (* p < 0.05).

According to Fig S2[†] in ESI, one month after transplantation of the new nanofibrous scaffolds, the implant was found to integrate well into the healthy host spinal cord: numerous cells stained by DAPI were detected throughout the implants. To assess axonal regeneration immunolabeling with GAP43, a marker for axonal growth, showed single fibers infiltrating the scaffold nanofibers. Fluorescent microscopy showed regenerating axons clearly visible in the conduits.

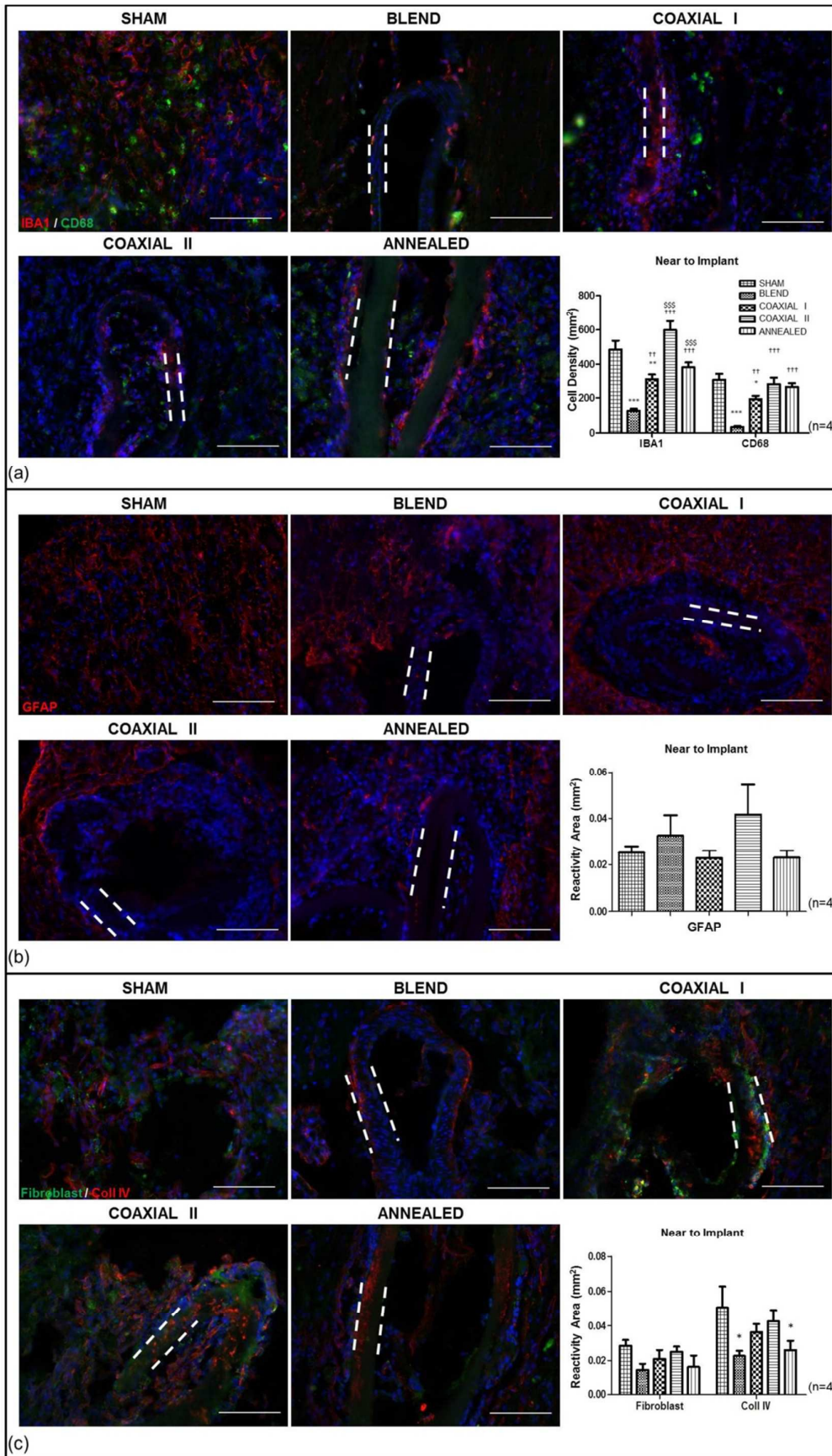


Figure 3 *In vivo* assays to evaluate tissue reaction in Sham-operated animals and those receiving Blend, Coaxial I, Coaxial II and Annealed scaffolds. Immunofluorescence staining for IBA1, CD68, GFAP, Fibroblast and Coll IV markers. Cell nuclei are visualized with DAPI (Blue). (a) IBA1+ (red) and CD68+ (green) cells were counted and the graph shows the density of cells near to implant. As for cell density (mm^2) near to implant the IBA1 quantification for all scaffolds was significantly different depending on the type of scaffold implanted (Sham vs Blend *** $p < 0.001$; Sham vs Coaxial I ** $p < 0.01$; Blend vs Coaxial I †† $p < 0.01$; Blend vs Coaxial II ††† $p < 0.001$; Blend vs Annealed ††† $p < 0.001$; Coaxial I vs Coaxial II \$\$\$ $p < 0.001$; Coaxial II vs Annealed \$\$\$ $p < 0.001$). Statistical differences for CD68+ cell density (mm^2) were similar to IBA1 (Sham vs Blend *** $p < 0.001$; Sham vs Coaxial I * $p < 0.05$; Blend vs Coaxial I †† $p < 0.01$; Blend vs Coaxial II ††† $p < 0.001$; Blend vs Annealed ††† $p < 0.001$). (b) Reactive area of GFAP+ cells (red) detected near to implant shows no significant difference among the experimental groups. Same methodology for (c) Fibroblast (green) and Coll IV (red) + cells. In case of Fibroblast marker the results show no statistical differences among all scaffolds; while, for Collagen IV, there were significant differences among Blend and Annealed vs Sham (* $p < 0.05$). Scale bar = 100 μm . Dashed lines outline scaffold walls.

3. Discussion

In the last decade, nanofibrous scaffolds entered the group of the most promising scaffolds for tissue engineering applications, providing novel alternative approaches for neural regeneration²¹.

Electrospinning is a promising technology for the fabrication of nano- and micro-fibrous scaffolds for tissue engineering²²⁻²⁴. Our previous studies showed that electrospun polymeric guidance channels loaded with functionalized SAPs, when transplanted into the cavity of chronic SCI, provided a significant ingrowth of newly formed nerve tissue among and within the guidance channels over a six-month period, fostering functional regeneration and behavioral recovery⁵.

Moving a step forward from nanofibrous polymeric microchannels, in current study we synthesized and characterized coaxial nanofibrous scaffolds made of polymers and SAPs with core-sheath structure using coaxial electrospinning. In this work PCL has been used as a flexible biopolymer to overcome the brittle properties of PLGA, in return PLGA improved the hydrophilicity of PCL²⁵ to enhance cellular adhesion²⁶. Nonetheless SAPs have already been shown to provide superior biochemical properties and biocompatibility, whereas lacking in user handling and spatial arrangement design tailorability. Incorporation of Ac-FAQ, a functionalized SAP with considerable neuroregenerative potential, aimed at improving cell adhesion and migration in case of neural tissue engineering¹². Therefore, in current study we compared the neuroregenerative potential of PCL-PLGA microchannels coaxially co-spun with encapsulated/emulsified SAPs. Reference materials include conventionally electrospun PCL-PLGA and an annealed coaxial sample. The SEM images (Fig. 1a) display in Coaxial I and Coaxial II samples with continuous and smooth cylindrical morphology, randomly oriented fibers with fairly uniform diameter. Annealed samples are characterized by fibers melted in patches and beads, but with a clearly visible porous structure.

Indeed in FTIR analysis, numbers of small peaks typical of peptides were detected in SAP blended scaffolds: these results clearly indicated that peptides were incorporated into nanofibers on Coaxial I and Coaxial II.

DSC indicates the electrospinning produces slightly less ordered crystals, with a more than 5 °C decrease in melting point compared to pure PCL, in the Blend and Coaxial I samples. This difference is not so intense to cause a decrease of the local

mechanical properties. However in the Coaxial II sample the decrease is more pronounced ($\approx 12^\circ\text{C}$): this should be considered in evaluating the performance of this material due to its reduced mechanical properties.

Biological response was evaluated by seeding mNSCs onto flat electrospun covered coverslips. At 7DIV in differentiating media mNSCs cultured on Coaxial I scaffolds showed spread and branched morphology comparable to those of Cultrex-treated wells, similar to adult neural cells evenly covering the scaffold top surfaces. Along this line no significant difference was detected between cells on Coaxial I and on Cultrex, obtaining values similar in the cell viability assay.

On the contrary smaller mNSCs populations were observed over Blend and Annealed scaffolds, with poorly branched round cell clusters, resembling immature mNSCs proliferated as neurospheres. In this case, MTS results showed significant differences compared to mNSCs on Cultrex. Instead mNSCs showed cell populations on Coaxial II with branched cell morphology similar to Coaxial I but not similar cell viability: this may be given by a not perfect coaxial spinning (burst effect of the water solvent used for the inner core) that, on the other hand, still kept most of the Ac-FAQ SAP within the inner core of the electrospun fibers²⁷. This result is probably due to the absence of adhesion sites surface coating on Blend, Annealed and Coaxial II scaffolds, whereas naturally derived materials, as Cultrex, contain biological adhesion proteins such as fibronectin and laminin.

On the other hand Coaxial I contains Ac-FAQ functionalized SAP in the outer shell that promotes mNSCs attachment, whereas Blend, Annealed and Coaxial II polymeric scaffolds lack specific cell adhesion sites²⁸.

Besides low cytotoxicity of the tested biomaterials, an ideal scaffold for stem cells transplantation in neural regenerative therapy should also coax the differentiation of NSCs to be transplanted²⁹. In this direction, we then assessed the phenotypes of differentiated mNSC progenies. In every scaffold, neuronal and glial phenotypes were present. Immunofluorescence imaging of neurons showed an organized network which resemble mature neurons obtained on Cultrex and in all scaffolds the percentage of Beta III Tubulin positive cells confirmed morphological observations.

The one-week differentiation of mNSCs on implants revealed that GFAP+ cells with star shaped were the dominant cell type in all circumstances, but in Blend and Annealed samples these glial cells significantly decreased with respect to Cultrex, probably due to the hydrophobic characteristic of PCL that leads to lower cell adhesion; therefore, the present studies demonstrate that Blend and Annealed scaffolds could discourage the mNSC differentiation into astrocytes, which is much desirable in therapy targeting SCI^{30, 31}.

In addition, with GalC/O4 markers the topography of Blend and Annealed samples is different: Blended nanofibres leads to reduction of cell population positive for GalC/O4 and this data is probably due to fibers diameter because Annealed scaffold presents thicker fibers compared to blend³².

One of the important goals of this study was to study host tissue response to the implantation of Coaxial scaffolds in healthy spinal cords. Macrophages are the primary cells of chronic inflammation and are known to be responsible for producing numerous biologically active agents to implanted biomaterials⁴. Macrophages interactions with foreign and implanted materials have been extensively reported in literature^{33, 34}.

Here scaffolds were implanted intramedullary and the overall histology showed good integration of all scaffolds into CNS without cavities between scaffolds and host-tissue.

Measures of the inflammation response to the implanted biomaterials were studied by activated microglia and macrophages responses. IBA1 – CD68 positive cells were found at 1 month in all cases including sham-operated tissue: largely as result of the incision surgery to the spinal cord during implantation.

IBA1 and CD68 cell density near to implant showed similar observations in sham-operated and in Coaxial II groups; but these results in comparison with Coaxial I sample showed significant differences, suggesting that Ac-FAQ functionalized SAP, contained in the shell, did not exacerbate the inflammatory response¹². By evaluating the cell density of IBA1+ and CD68+ cells within implant walls we demonstrated that in the Annealed scaffolds there was a significant reduction of IBA1+ cells in respect to the others given by fused fibers hampering cell infiltration. In all wall scaffolds the activated macrophages (CD68+ cells) are less than IBA1+ cells, indicating that these scaffold when implanted into the spinal cords elicit a foreign body response similar to conventional Blend scaffolds⁵. GFAP positive reactive astrocytes were also present around the implants. The post-surgery response of astrocytes is characterized by hyperplasia and hypertrophy of cell bodies^{35,36}. Some studies demonstrated that astrocytes positively influence the neural repair process: they facilitate neuronal sprouting^{37,38} and exert a cytotropic effect on neurons through the secretion of growth factors and guidance molecules^{38,39}. The majority of the GFAP reactivity was attributed to the surgery and not as a direct effect of the implanted biomaterials because there weren't significant differences among Sham-operated and all other experimental groups.

Lastly we studied immunofluorescence staining for Collagen IV, one the main structural components of basement membrane in the nervous system. In our previous study, Collagen IV deposition have been detected both nearby and within the conduit inner walls in concurrence with regenerated fibers⁴⁰. The reactivity area positive for Collagen IV in Coaxial I and Coaxial II near to implant had values comparable with data obtained in Sham group. These values suggest the preservation of a permissive microenvironment for the regeneration of CNS tissue. On the other hand, the amount of Collagen IV was significantly lower in case of Blended and Annealed nanofibers. These studies clearly demonstrated the superiority of SAP blended/encapsulated coaxial nanofiber scaffolds.

Based on these facts, *in vivo* results show that Coaxial I displays immune response lower than sham-operated group and the highest NSC viability *in vitro*.

Using GAP43 antibody, we found many axons growing inside the implants along the biomaterial conduits: some of those co-localized with SMI31 immunostaining.

The biofunctionalization with the FAQ motif has improved NSC cultures as expected but may also have improved interactions with host tissues by simply displaying the peptide functional motifs. This seems to favor Coaxial I as a scaffold for nervous regeneration, in particular if NSC transplantation is considered part of the multi-disciplinary therapeutic approach.

Coaxial techniques show great potential for controlled drug delivery applications and, supported by our results, can be further improved with emulsifications of functionalized SAPs to be used in the field of regenerative medicine with various applications such as promoting nerve regeneration in SCI⁵.

4. Conclusion

Functionalization and spatial orientation of ECM mimicking nanofibers is desirable for neural tissue regeneration. Therefore we here reported the functionalization of electrospun nanofibrous microchannels for SCI. Blending and encapsulation of functionalized self-assembling peptides via coaxial electrospinning circumvented the use of chemical cross-linking or immobilization reactions for specific biofunctionalizations. The smooth and continuous coaxial nanofibers did not show any significant change in surface as well as bulk properties due to incorporation of SAPs. On the other hand *in vitro* and *in vivo* studies showed profound effect due to SAPs incorporation. In *in vitro* experiments NSCs were used for their potential use in neural tissue engineering as well as their ability to differentiate into various neural cells⁴¹⁻⁴³. Our results proved promising interactions of the tested scaffolds with cells from the CNS. On the other hand *in vivo* experiments showed a satisfactory low host response to the novel implants, thus paving the way to their application in experiments for the regeneration of the chronic SCI in the near future⁵.

5. Method

Ac-FAQ was synthesized as previously described¹². PLGA, (75:25, MW 66000-107000) and PCL (MW 80000) were purchased from Sigma Aldrich, USA. Chloroform and Methanol (HPLC grade) solvents used for electrospinning were obtained from VWR.

5.1 Fabrication of microfibrous meshes and microchannels

The electrospinning setup used in this study was designed specifically for this project and consisted of a syringe pump (NewEra pump system Inc, USA), a high voltage power supply (Spellman, USA), a copper plate for collection of fibers on glass cover slips and an adjustable rotatory mandrel for microchannel fabrication. For coaxial electrospinning a coaxial needle was purchased from Ramehart, USA with the following diameters: Shell needle: 0.8192 mm (outer diameter) and 0.51 mm (inner diameter), Core needle: 0.4636 mm (outer diameter) and 0.260 mm (inner diameter). The 9.5% w/w PCL (5.5 % w/w) + PLGA (4 % w/w) polymer solution was prepared in 3:1 chloroform and Methanol solution. PCL/PLGA solution was prepared 24 hours prior to experiment. Before experiment an emulsion with Ac-FAQ were prepared with PCL-PLGA solution. A 33G micro needle (Hamilton needle, outer diameter=200 μ m) as target was fixed in rotating arm of mandrel and grounding electrode (8 mm copper plate) was placed just below the needle and connected with grounding cable. The polymer solutions were loaded in syringe and mounted on syringe pump. A co-axial needle was connected with both syringes. Before electrospinning the mandrel was turn on and inspected for

possible contact between rotating needle and ground electrode. After confirming the alignment of needle and non contact mode with copper plate the power supply was turn on. A detailed description is provided in Table 1.

5.1.1 Blend

The polymer solution of PCL-PLGA was loaded in syringe and a standard needle was used. The distance between the needle tip and the collector plate/mandrel was set at 30 cm. The voltage applied between electrodes was set at 1 kV/cm. For *in vitro* studies pre-sterilized glass coverslips (diameter 1 cm²) were fixed on collector plate for homogenous deposition of fibers. For microchannel fabrication, the nanofibers were deposited on the 0.200 mm diameter micro needle target fixed on edge of rotatory mandrel and set at 30 rpm. After deposition that micro needle was carefully removed, leaving a hollow conduit for further analysis.

5.1.2 Coaxial I

Pre-dissolved polymer and peptide solutions were mixed in ratio of 1000 μ l: 200 μ l and vortexed for 5 minutes. The partial miscibility of polymeric solvent (chloroform and Methanol) with peptide solvent (water) facilitated the equal distribution of peptide solution into polymeric. A milky white emulsified solution with low viscosity was obtained after 5 minutes of vortexing. Emulsified solution and polymer solution were loaded in separate syringes and connected to coaxial needle with silicon tubes. The core solution i.e. peptide polymer emulsion was pumped at 0.05 ml/min, whereas shell solution i.e. PCL-PLGA at 0.1 ml/min. The distance between the needle tip of the syringe and the collector plate/mandrel was set at 30 cm. The voltage applied between electrodes was set at 1 kV/cm. For *in vitro* studies pre-sterilized glass coverslips (diameter 1 cm²) were fixed on collector plate for homogenous deposition of fibers. For microchannel fabrication Hamilton needle was used as a target and fixed on edge of rotatory mandrel and set at 30 rpm.

5.1.3 Coaxial II

Polymer and peptide solution were loaded in separate syringes and connected to a coaxial needle with help of silicon tubing. The core solution, i.e. peptide, was pumped at 0.05 ml/min whereas shell solution i.e. PCL-PLGA at 0.1 ml/min. The remaining electrospinning parameters and process details for microchannel remain similar to Coaxial I.

5.1.4 Annealed nanofibrous microchannel

The PCL-PLGA microchannel was prepared as described earlier. After fabrication channels were dip into distilled water set at 60 °C for 10 seconds and then immediately quenched into ice-cold water.

All samples (mesh and microchannels) were lyophilized for 48 hours after synthesis and used for further experiments.

Peptide stability was verified via electro-spraying and subsequent HPLC and LC-MC tests (see ESI and Fig S3† for details).

5.2 Scanning Electron Microscopy

The fiber diameter and surface morphology were characterized using a scanning electron microscope (SEM), (Tescan, Czech Republic). A representative section of the deposited microfibrinous matrix was sputter-coated with gold and was observed under the SEM at a working distance of 10 mm and an accelerating voltage of 20 kV.

5.3 Water contact angle measurement

The change in PCL-PLGA nanofibrous hydrophobicity was measured by contact angle relaxation of water droplet by sessile drop method using a contact angle goniometer (OCA 15EC Dataphysics). After lyophilization the 1x1 cm electrospun matrix was then attached to a silicon wafer for contact angle measurements. Three samples were used for each category and two measurements were performed on each sample. Therefore, the average of six measurements for each category was used for current study. In each measurement, a droplet of deionized water (4 μ l) was pipetted onto the membrane surface. Images of the water droplet were taken using a high-speed digital camera and circular fitting method has been used for contact angle measurement (see ESI and Fig S4† for details). All contact angle measurements were performed at 25 °C and baseline was corrected manually.

5.4 Fourier transforms infrared spectroscopy

In order to characterize the nanofibrous surface and peptide integration ATR-FTIR spectroscopy was conducted using a PerkinElmer (Spectrum 100) FTIR spectrometer. Control of the instrument as well as collection and primary analysis of data was accomplished using inbuilt Spectrum version 6.3.2. Prior to data acquisition, the optical bench was purged with dry N₂ to minimize external interference. For each run, a total of 60 scans were collected at a resolution of 4 cm⁻¹. In order to minimize the possibility of error, the FTIR spectra of all samples were recorded at least three times at random location. Each recorded spectrum was corrected for background (atmospheric components). All spectra were recorded at 25 °C.

5.5 Thermal analysis

Differential scanning calorimetry (DSC) analysis was performed on a Mettler-Toledo DSC 1 under dynamic nitrogen atmosphere (80 mL min⁻¹), using 6-8 mg of sample contained in a 40 μ L aluminum pan. Blend, Coaxial I and Coaxial II nanofibrous films were analyzed with a three-step program. A first heating ramp from -100 °C to 200 °C with 20 °C/min was followed by cooling at 20 °C/min and by a second heating from -100 °C to 200 °C with 20 °C/min. Enthalpy associated to phase transitions was measured by integrating the relevant peaks with the STARE software. All experiments were conducted in triplicates. The DSC cell was calibrated with indium (melting point 156 °C) and zinc (melting point 419.4 °C) standards. As reference, pure PCL and PLGA pellets were also analyzed.

5.6 Scaffold preparation for *in vitro* and *in vivo* tests

In vitro tests scaffold were electrospun onto glass coverslips while microchannels were obtained for *in vivo* experiments (see “Fabrication Section”). Circular glass coverslips were sterilized using UV radiation for 1 h and washed three times with sterile PBS for 15 minutes; instead, electrospun microchannels, soaked in PBS, were sterilized using UV radiation for 1 h and then they were used for *in vivo* implants.

5.7 NSC Cultures

Neural Stem Cell cultures were established and expanded as previously described . Briefly, murine NSC (mNSC) were isolated from the Subventricular Zone (SVZ), a Subependymal region of the Lateral Ventricles of 8-week-old CD-1 albino mice striata and cultured till passage 10.

In vitro tests were performed adapting the procedure previously described by authors ¹⁰. mNSCs were cultured to a neurosphere state and at passage 10 they were mechanically dissociated and, on the day after, seeded onto electrospun circular glass coverslips at a density of 3×10^4 cells / well (1 cm^2). For both viability and differentiation tests, basal medium supplemented with β FGF (10 ng/ml) has been used. After 2 days *in vitro* (DIV), the medium was changed with a medium containing Leukemia Inhibitory Factor (LIF, Chemicon) (20 ng/ml) and Brain Derived Neurotrophic Factor (BDNF, Peprotech) (20 ng/ml) to pursue the neuronal and glial population maturation in NSC progeny. For both viability and differentiation assays positive control consisted of Cultrex-BME[®] substrate (R&D systems) diluted in basal medium (1:100).

5.7.1 Cell proliferation assay

To assess the viability of mNSCs seeded on scaffolds, the Cell Titer 96[®]Aqueous One Solution Cell Proliferation assay (MTS assay) was used.

To study the cell proliferation on different electrospun scaffolds, viable cells were quantified by using the colorimetric MTS assay, this reagent contains a tetrazolium compound that is bio-reduced by cells into a colored formazan product, this conversion is produced by metabolically active cells. After 7 days of cell seeding in 48 – well plate, cells were incubated with a 20% solution of MTS reagent. After 1 h of incubation at 37 °C in 5 % CO₂, aliquots were pipetted into 96 multiwell plates. The absorbance of each sample, directly proportional to the number of live cells, was measured at 490 nm using a spectrophotometric microplate reader (Sinergy H1 Hybrid Multi-Mode Microplate Reader, Bio Tek).

5.7.2 Characterization of differentiated NCS progeny

To perform immunofluorescence tests cells at 7DIV were fixed with paraformaldehyde 4% (PFA4%) and the following primary antibodies were used: rabbit anti-GFAP (1:500, DakoCytomation), mouse anti-Beta III Tubulin (1:500, Covance), mouse anti-GalC (1:200, Chemicon) and anti-O4 (1:200, Chemicon). Secondary antibodies were goat anti-Mouse Alexa 488 (1:1000, Molecular

Probes), goat anti-Mouse Cy3 (1:1000, Jackson Immunoresearch), goat anti-Rabbit Cy3 (1:1000, Jackson Immunoresearch). Cell nuclei were counterstained with DAPI (Molecular Probes). Quantitative analyses were performed by counting 100–300 cells for each of 9 randomly chosen for each independent experiment. Fluorescence images of the adhering cells were acquired by inverted fluorescence microscope, via Zeiss microscopes Axioplan 2 and ApoTome System.

5.8 Microchannels implantation into rodent spinal cord tissue (experimental design)

15 adult female Sprague-Dawley (SD) rats were used. All procedures were carried out with protocols approved by Institutional Animal Care and Use Committee of the University of Milan-Bicocca (IACUC 130/2014-B) and were performed according to EC guidelines (86/609/EEC), to the Italian legislation on animal experimentation (Decreto L.vo 116/92).

The animals (Harlan Laboratories, Italy) (250~ 275 g) were housed 2-3 rats for cage, given free access to food and water, and kept on a 12/12 h light/dark cycle.

The implantation surgeries were performed under strict sterile conditions. For implantation, rats were deeply anesthetized with an intraperitoneal injection of ketamine (80 mg kg⁻¹) and xylazine (10 mg kg⁻¹). When unresponsive to toe pinch, the dorsal was shaved following incision of the dorsal skin, a dorsal laminectomy was performed to expose the dura overlying the spinal cord at thoracic level T9 – T10.

The vertebral column was stabilized by clamping the column at vertebra T8 and T11. Longitudinal incisions were made into the dura and the underlying spinal cord at 1 mm lateral to either side of the midline (Sham group). Offset between the two incisions was 5 mm. 2 microtubes (1-mm in length) of the same typology were inserted into each of the two incision sites (Treated group) at thoracic level T9 – T10. We tested the following microchannels: Blend, Coaxial I, Coaxial II and Annealed. We chose to implant two types of microchannels for animal in far apart incision sites along the spinal cord in order to minimize the animal sacrifice: we also rotated the couple of each type of implants for animal.

Following implantation, the overlying muscle and skin were closed with vicryl sutures and metal clips, respectively.

Animals were monitored after the implantation for one month and no significant behavioral changes or other adverse were observed. Rats were treated daily for one week with analgesic (carprofen, 5 mg kg⁻¹) and antibiotic (enrofloxacin, 5 mg kg⁻¹).

5.8.1 Immunohistochemistry

Four weeks after implantation, rats were deeply anesthetized with an overdose of avertin (400 mg/kg).

Animals were sacrificed by cardiac perfusion under terminal anesthesia using PFA 4%. Once removed, spinal cord were post fixed overnight in PFA 4% and tissues were cryopreserved in 30% sucrose and cut on a frozen blade cryostat into 16- μ m thick longitudinal sections. Sections were cut serially, three per glass.

For staining of macrophages and microglia, slices were washed with PBS, permeabilized with 0.1% Triton X-100 and treated with 10% normal goat serum (NGS). We used the following primary antibodies: mouse anti-CD68 (1:500, Serotec), rabbit anti-IBA1 (1:1000, Wako).

For immunofluorescence analysis of gliosis, we used mouse-anti glial fibrillary acidic protein (GFAP) (1:500, Millipore). For immunofluorescence staining of basement membrane, we used rabbit anti-Collagen IV (1:100, Cedarlene), mouse anti-Fibroblast (1:400, Acris).

For axonal regeneration analysis, immunohistochemistry was performed with rabbit-anti growth associated protein-43 (GAP-43) (1:100, Chemicon). Finally, mouse-anti-SMI-31 (1:1000, Covance) was used to analyze phosphorylated neurofilament.

To reveal primary antibodies we used the following secondary antibodies: goat anti-rabbit Cy3 (1:1000, Jackson) and goat anti-mouse Alexa 488 (1:1000, Invitrogen). Sections were counterstained with DAPI and mounted with FluorSave reagent (Calbiochem).

To standardize the results, all measurements were made from digital pictures taken on a Zeiss Apotome microscope at 20X magnification and performed via ImageJ software. Cell density for IBA1 and CD68 markers was evaluated near to implant and within the implant wall. Quantification of GFAP reactivity area on implant site was performed on longitudinal sections using ImageJ software. The color images of the implant site of cells positive to GFAP were converted into binary images; areas were quantified by measuring the number of positive pixels. Pixel area was converted to mm^2 and measurements were averaged over all sections per animal in order to quantify the reactivity area of each scaffold per each animal. The same methodology was chosen for Fibroblast and Collagen IV markers.

5.9 Overall Statistical Analysis

Data were processed using GraphPad Prism 5 software. Contact angle measurements were analyzed using One-Way ANOVA and subsequent Tukey HSD Post-hoc Test. Values are reported as means \pm standard error of the mean (SEM). In the *in vitro* study, MTS assay was analyzed via one-way ANOVA followed by Dunnett's Multiple Comparison Test; Beta III Tubulin and GFAP were evaluated by two-way ANOVA followed by Bonferroni post-test; GalC - O4 was performed via one-way ANOVA followed by Dunnett's Multiple Comparison Test. In the *in vivo* study, IBA1/CD68 and Fibroblast/Collagen IV significance tests were carried out by two-way ANOVA followed by Bonferroni post-test; finally GFAP marker was analyzed by one-way ANOVA followed by Tukey's Multiple Comparison Test.

Acknowledgments

This work was supported by Fondazione Cariplo, grant no. 2011-0352, by Vertical Onlus and by the "Ricerca Corrente 2011" funding granted by the Italian Ministry of Health and by the "5x1000" voluntary contributions.

References

1. C. H. Tator and M. G. Fehlings, *J Neurosurg*, 1991, **75**, 15-26.
2. A. Raspa, G. A. A. Saracino, R. Pugliese, D. Silva, D. Cigognini and V. A. a. G. F., *Advanced Functional Materials*, 2014, **24**, 6317–6328,.
3. D. F. Williams, *Biomaterials*, 2008, **29**, 2941-2953.
4. J. M. Anderson, A. Rodriguez and D. T. Chang, *Semin Immunol*, 2008, **20**, 86-100.
5. F. Gelain, S. Panseri, S. Antonini, C. Cunha, M. Donega, J. Lowery, F. Taraballi, G. Cerri, M. Montagna, F. Baldissera and A. Vescovi, *ACS Nano*, 2011, **5**, 227-236.
6. W. J. Li, C. T. Laurencin, E. J. Caterson, R. S. Tuan and F. K. Ko, *J Biomed Mater Res*, 2002, **60**, 613-621.
7. M. Shin, O. Ishii, T. Sueda and J. P. Vacanti, *Biomaterials*, 2004, **25**, 3717-3723.
8. X. Zong, K. Kim, D. Fang, S. Ran, B. S. Hsiao and K. Chu, *Polymer*, 2002, **43**, 4403–4412.
9. D. H. Reneker, W. Kataphinan, A. Theron, E. Zussman and A. L. Yarin, *Polymer*, 2002, **43**, 6785–6794.
10. F. Gelain, D. Bottai, A. Vescovi and S. Zhang, *PLoS One*, 2006, **1**, e119.
11. G. A. Silva, C. Czeisler, K. L. Niece, E. Beniash, D. A. Harrington, J. A. Kessler and S. I. Stupp, *Science*, 2004, **303**, 1352-1355.
12. F. Gelain, D. Cigognini, A. Caprini, D. Silva, B. Colleoni, M. Donega, S. Antonini, B. E. Cohen and A. Vescovi, *Nanoscale*, 2012, **4**, 2946-2957.
13. F. Zamani, M. Amani-Tehran, M. Latifi and M. A. Shokrgozar, *J Mater Sci Mater Med*, 2013, **24**, 1551-1560.
14. J. Xie, M. R. MacEwan, A. G. Schwartz and Y. Xia, *Nanoscale*, 2010, **2**, 35-44.
15. Y. Z. Zhang, X. Wang, Y. Feng, J. Li, C. T. Lim and S. Ramakrishna, *Biomacromolecules*, 2006, **7**, 1049-1057.
16. H. Jiang, Y. Hu, Y. Li, P. Zhao, K. Zhu and W. Chen, *J Control Release*, 2005, **108**, 237-243.
17. H. Jiang, Y. Hu, P. Zhao, Y. Li and K. Zhu, *J Biomed Mater Res B Appl Biomater*, 2006, **79**, 50-57.
18. Z. Sun, E. Zussman, A. L. Yarin, J. H. Wendorff and G. A., *Advanced Materials*, 2003, **15**, 1929–1932.
19. C. L. He, Z. M. Huang, X. J. Han, L. Liu, H. S. Zhang and L. S. Chen, *Journal of Macromolecular Science*, 2006, **45**, 515-524.
20. Z. G. Tang, J. T. Callaghan and J. A. Hunt, *Biomaterials*, 2005, **26**, 6618-6624.
21. H. Cao, T. Liu and S. Y. Chew, *Adv Drug Deliv Rev*, 2009, **61**, 1055-1064.
22. M. M. Stevens and J. H. George, *Science*, 2005, **310**, 1135-1138.
23. P. X. Ma, *Adv Drug Deliv Rev*, 2008, **60**, 184-198.
24. T. Dvir, B. P. Timko, D. S. Kohane and R. Langer, *Nature Nanotechnology*, 2011, **6**, 13-22.
25. J. Y. Kim and D. W. Cho, *Microelectronic Engineering*, 2009, **86**, 1447-1450
26. N. T. Hiep and B. T. Lee, *J Mater Sci Mater Med*, 2010, **21**, 1969-1978.
27. Y. Su, X. Li, Y. Liu, Q. Su, M. L. Qiang and X. Mo, *J Biomater Sci Polym Ed*, 2011, **22**, 165-177.
28. F. Gelain, A. Lomander, A. L. Vescovi and S. Zhang, *J Nanosci Nanotechnol*, 2007, **7**, 424-434.

29. J. R. Thonhoff, D. I. Lou, P. M. Jordan, X. Zhao and P. Wu, *Brain Res*, 2008, **1187**, 42-51.
30. J. Silver and J. H. Miller, *Nat Rev Neurosci*, 2004, **5**, 146-156.
31. Z. Su, W. Niu, M. L. Liu, Y. Zou and C. L. Zhang, *Nat Commun*, 2014, **5**, 3338.
32. G. T. Christopherson, H. Song and H. Q. Mao, *Biomaterials*, 2009, **30**, 556-564.
33. Q. Zhao, N. Topham, J. M. Anderson, A. Hiltner, G. Lodoen and C. R. Payet, *J Biomed Mater Res*, 1991, **25**, 177-183.
34. J. M. Anderson, *Annu. rev. mater. Res.*, 2001, **31**, 81-110.
35. D. Stanic, W. Tripanichkul, J. Drago, D. I. Finkelstein and M. K. Horne, *Brain Res*, 2004, **1023**, 83-91.
36. C. L. Parish, D. I. Finkelstein, W. Tripanichkul, A. R. Satoskar, J. Drago and M. K. Horne, *J Neurosci*, 2002, **22**, 8034-8041.
37. D. R. Nisbet, K. E. Crompton, M. K. Horne, D. I. Finkelstein and J. S. Forsythe, *J Biomed Mater Res B Appl Biomater*, 2008, **87**, 251-263.
38. P. E. Batchelor, G. T. Liberatore, J. Y. Wong, M. J. Porritt, F. Frerichs, G. A. Donnan and D. W. Howells, *J Neurosci*, 1999, **19**, 1708-1716.
39. P. E. Batchelor, M. J. Porritt, P. Martinello, C. L. Parish, G. T. Liberatore, G. A. Donnan and D. W. Howells, *Mol Cell Neurosci*, 2002, **21**, 436-453.
40. S. Panseri, C. Cunha, J. Lowery, U. Del Carro, F. Taraballi, S. Amadio, A. Vescovi and F. Gelain, *BMC Biotechnol*, 2008, **8**, 39.
41. J. L. McBride, S. P. Behrstock, E. Y. Chen, R. J. Jakel, I. Siegel, C. N. Svendsen and J. H. Kordower, *J Comp Neurol*, 2004, **475**, 211-219.
42. K. Chu, M. Kim, K. I. Park, S. W. Jeong, H. K. Park, K. H. Jung, S. T. Lee, L. Kang, K. Lee, D. K. Park, S. U. Kim and J. K. Roh, *Brain Res*, 2004, **1016**, 145-153.
43. S. Pluchino, A. Quattrini, E. Brambilla, A. Gritti, G. Salani, G. Dina, R. Galli, U. Del Carro, S. Amadio, A. Bergami, R. Furlan, G. Comi, A. L. Vescovi and G. Martino, *Nature*, 2003, **422**, 688-694.